Flame pyrolysis prepared catalysts for the steam reforming of ethanol

Matteo Compagnoni[1], Josè Lasso F.[1], Alessandro Di Michele[2] and Ilenia Rossetti[1,*]

[1]Dip. Chimica, Università degli Studi di Milano, INSTM Unit Milano-Università and CNR-ISTM, via C. Golgi, 19, I-20133 Milano, Italy

[2]Dip. di Fisica - Università degli Studi di Perugia, Via Pascoli, 06123 Perugia

** Corresponding author: Fax +39-02-50314300; email: ilenia.rossetti@unimi.it*

Abstract

An innovative flame pyrolysis method has been employed for the preparation of Ni-based catalysts for the steam reforming of ethanol. Titania and lanthana supports, characterized by variable acidity and Ni loading have been compared, as well as different procedures to add the Ni active phase to the support, affecting metal dispersion. Samples characterization evidenced that the one pot preparation of the catalyst by flame pyrolysis resulted in the formation of a mixed oxide phase and, thus, in higher Ni dispersion even at the highest loading. The metal-support interaction was also strengthened when preparing the samples by FP than by conventional impregnation.

Steam reforming at 750°C resulted in full ethanol conversion without byproducts, so that a fuel processor able to feed a 5 kW_e + 5 kW_t fuel cell may operate with *ca*. 1.35 kg of catalyst. Tests at lower temperature were also carried out, focusing on the optimization of the resistance to coking.

The best results at 500°C were achieved for the FP-prepared sample supported over La_2O_3 and containing 15 wt% Ni as active phase.

Keywords: Ethanol steam reforming; Ni-based catalysts; Resistance to coking; Flame pyrolysis.

1. Introduction

A general look to the energetic world situation could suggest the importance to foster the production of energy from non-traditional sources. The increasing demand of energy due to the impressive industrialization in many countries, the evident reduction of fossil fuel reserves, the influence of anthropogenic emissions contributing to the climate change, led to a growing international pressure to the conservation of the environment.

The production of energy through sustainable processes has been often focused on H_2 as energy vector [1–4]. Among the methods to produce H_2, Steam Reforming (SR) is one of the most common and feasible [5–12]. The use of raw materials from biomass may be considered for H_2 production with neutral carbon balance, even though detailed life-cycle assessment is compulsory [13]. In this order, bioethanol is nowadays very attractive, given the fact that it is the most available biofuel worldwide and, as second generation biofuel, it does not affect the production of food and feed. Low concentration solutions are acceptable for steam reforming, given the need of steam cofeeding, whereas they are not suitable for different applications, such as combustion. This is even more important because the anhydrification of bioethanol represents one of its major production costs. Therefore, diluted bioethanol may be attractive from an economical point of view [14,15], provided that it does not contain poisons depressing catalytic activity.

Many examples of catalytic materials for this application can be found in the literature. Verykios et al. studied H_2 production by SR of bioethanol at first focusing on Ni as active phase loaded on different supports [16,17] and on supported noble metals [18]. Different Co-based catalysts have been proposed as active and stable for H_2 production [19–22]. Nonetheless, Ni commonly showed higher catalytic activity in activating the C-C bond [23–26],

in addition to a better control of the active phase dispersion. Other papers on Ethanol SR (ESR) report that it is possible to limit coke formation and to lower the reaction temperature, especially by finely tuning catalyst formulation and the metal-support interaction [24,27,28].

One challenge for SR at high temperature is catalyst deactivation by sintering, so that high thermal resistance of the catalytically active material is a pressing need. On the other hand, it is envisaged to operate SR at lower temperature, to decrease the heat input to the reactor with the aim of process intensification. Nevertheless, at low temperature catalyst deactivation may be impressive by coking, due to the formation of carbon filaments, and occurs mainly over big Ni and Co particles [11]. The evolution of filamentous C and its correlation with ethanol conversion and byproducts at 500°C has been recently addressed [29] and the mechanism of formation, mainly from CO and CH_4 has been detailed [21,30].

Additional coking may occur over acidic sites of the support. Acidity can be limited by using intrinsically basic oxides or by titrating surface acidity by using a basic promoter [29,31–35]. For instance, CaO was used to tune ZrO_2 acidity [36]. In such case, Ca^{2+} substituting for Zr^{4+} in the framework additionally induced the formation of oxygen vacancies, which helped oxydrils activation, with further improvement of the resistance to coking. Lanthana was very often used as a mean to limit support acidity for this application [29,32,34,35,37–41]. Therefore, an appropriate catalyst formulation should be found, which allows to reach the highest catalytic performance together with proper resistance to deactivation. To date, it is suggested to operate with very well dispersed active metals, properly stabilized at high temperature through strong interactions with the support (having limited or nil acidity).

The Flame Spray Pyrolysis (FP) technique [42–47] proved able to prepare catalysts with high surface area, usually connected with high catalytic activity, and good thermal stability. High dispersion of the active phase can be achieved in principle, which may improve catalyst resistance to coking. Thus this preparation technique may help solving both stability problems related to sintering and coking.

Therefore, the aim of this work was the demonstration of the features of FP prepared catalysts for the SR of ethanol, in order to address the key stability issues for this application at both high and low temperature. This is an innovative synthesis procedure for this specific application, and already proved interesting to prepare catalysts for the steam reforming of methanol [48,49] and glycerol [50]. A set of catalysts was synthesized one-pot by flame pyrolysis and compared with another set prepared by impregnation of the active phase on the FP-prepared support. This high temperature synthesis was adopted to impart suitable thermal resistance to the samples and to provide a good metal dispersion and a high metal support interaction, which indeed showed a pivotal importance to improve resistance towards coking. Two supports were also compared, *i.e*. TiO_2 and La_2O_3, characterized by different surface acidity and redox properties, as well as different Ni loading. All the catalysts were characterized by various techniques, X ray powder diffraction (XRPD), N_2 physisorption, scanning electron or transmission microscopy (SEM-TEM-EDX), temperature programmed reduction (TPR). The activity testing was done in a home-made micro-pilot plant for ethanol steam reforming under different process conditions.

2. EXPERIMENTAL

2.1. Catalysts preparation

TiO_2 was prepared from titanium isopropoxide (Aldrich, purity 97%) dissolved in o-xylene (Aldrich, purity 97%) with a 0.1 mol/L final concentration referred to TiO_2.

La_2O_3 was produced from lanthanum acetate (Aldrich, purity 99,9%), dissolved in propionic acid (Aldrich, purity 97%) and diluted with o-xylene (1:1 vol/vol) achieving a final concentration of 0.1 mol/L referred to La_2O_3.

The solutions were fed to the home-designed FP burner [45] with 2.2 ml/min flow rate and 1.5 bar pressure drop across the nozzle. The latter was co-feed with 5 L/min of O_2.

In case of catalysts prepared in one-step by FP the active metal has been directly incorporated during the support synthesis. Ni was added to the above mentioned mother solutions by dissolving Ni acetate (Aldrich, purity 98%) in propionic acid. Nominal Ni loading was 5, 10 and 15 wt% on both supports. A perovskitic catalyst precursor ($LaNiO_3$) was also prepared, for which the mother solution was prepared with a La/Ni ratio = 1 (mol/mol), labelled in the following as LaNi-F. The same catalyst formulations were prepared by using the FP-synthesised bare TiO_2 and La_2O_3 and by adding Ni through wet impregnation with and aqueous solution of $Ni(NO_3)_2$.

The catalysts were reduced post synthesis for 1h at 800°C in a 20 vol% H_2 / N_2 gas mixture. Sample codes in Table 1 are denoted as x-Ni/y-z, where x represents Ni wt%, y is T for TiO_2 and La for La_2O_3 supports respectively, z = F or I for samples prepared in one step by FP or with Ni added by impregnation on the FP-prepared support.

2.2 Catalysts characterization

X-rays diffraction (XRD) analysis was performed on a Phillips PW3020 instrument. Specific surface area and pore size distribution were evaluated through the collection of N_2 adsorption-desorption isotherms at 77K on a Micromeritics ASAP 2010 instrument. Surface area was calculated on the basis of the Brunauer, Emmet and Teller equation (BET). Prior to the analysis the samples were outgassed at 300°C overnight.

Scanning electron microscopy (SEM) has been carried out using a Philips XL-30CP instrument and the surface and elemental composition of the catalysts was determined using energy dispersive X-ray analysis (EDX). The scanning electron microscope was equipped with a LaB6 source and an EDAX/DX4 detector. The acceleration potential voltage was maintained between 15 keV and 20 keV and samples were metallized with gold.

Transmission electron microscopy (TEM) was performed with a Philips XL-30CP electron microscope.

Temperature programmed reduction (TPR) was performed by placing the catalyst in a quartz reactor and heating by 10°C/min from 25 to 800°C in a 5 vol% H_2/Ar stream flowing at 40 mL/min. H_2 consumption was monitored continuously by means of a mass spectrometer (MS).

2.3 Ethanol steam reforming (ESR)

Activity tests were performed by means of a micro pilot plant constituted by an Incoloy 800 continuous downflow reactor heated by an electric oven. The reactor temperature was controlled by an Eurotherm 3204 TIC. The reactor may be fed both with liquid and gaseous reactants and at the reactor outlet there is trap for the collection of possible liquid products and a gas sampling point.

The catalysts were pressed, ground and sieved into 0.15-0.25 mm particles. Ca. 0.5 g were loaded into the reactor after dilution 1:3 (vol/vol) with SiC of the same particle size. Catalyst activation was accomplished by feeding 50 cm^3/min of a 20 vol% H_2/N_2 gas mixture, while heating by 10 °C/min up to 800 °C, then kept for 1 hour. During activity testing 0.017 cm^3/min of a 3:1 (mol/mol) H_2O:CH_3CH_2OH liquid mixture were feed to the reactor by means of a HPLC pump (Waters, mod. 501). The mixture was vaporized at the reactor inlet and added with 56 cm^3/min of N_2, used as internal standard for GC analysis, and 174 cm^3/min of He. Such dilution of the feed stream was calibrated so to keep the reactants mixture in the vapor phase even at zero conversion at the reactor outlet. The activity tests were carried out at atmospheric pressure, GHSV=2500 h^{-1} (referred to the ethanol + water gaseous mixture) at 500, 625 and 750 °C. The analysis of the out-flowing gas was carried out by a gas chromatograph (Agilent, mod. 7980) equipped with two columns connected in series (MS and Poraplot Q) with a thermal conductivity detector (TCD), properly calibrated for the detection of ethanol, acetaldehyde, acetic acid, water, ethylene, CO, CO_2, H_2. Material balance on C-containing products was checked to account for coke deposition. Repeated

analyses of the effluent gas were carried out every hour and the whole duration of every test at each temperature was *ca*. 8h. The data reported in the Tables are averaged between 4 and 8 h-on-stream, if not else specified.

The raw data, expressed as mol/min of each species outflowing from the reactor, have been elaborated to give the following parameters:

Products distribution: Y_i= mol i/$\sum$ (mol i) (E1)

C balance: 100- (((molCH_3CH_2OH*2)$_{in}$-$\sum$(mol C_i*α_i)$_{out}$)/(molCH_3CH_2OH*2)$_{in}$)*100 (E2)

Conversion: X_i= (mol i_{in}-mol i_{out})/mol i_{in} , with i=H_2O, CH_3CH_2OH (E3)

Selectivity: S_i= (mol i/ν_i)(mol ethanol$_{in}$ - mol ethanol$_{out}$) (E4)

H_2 productivity: mol H_2 out/min kg_{cat} (E5)

Where *i* = products detected, dry basis; α_i= number of C atoms in the *i-th* molecule; $\nu_{i=}$ stoichiometric coefficient of species *i* in the ESR reaction.

3. Results and discussion

We selected flame pyrolysis as a new mean for the preparation of SRE catalysts due to the possibility to impart high thermal resistance to the prepared samples during the high temperature synthesis. This is important during testing at high temperature (>600°C) in order to achieve suitable resistance to sintering. It is also important at lower temperature thanks to the intimate contact between Ni and the active phase and strong metal-support interaction possibly achievable through this synthesis procedure. This may be important to improve resistance to coking by keeping Ni well dispersed. In order to check these features we focused on two different supports. TiO_2 proved interesting during previous investigations [28,50], so here we tuned Ni loading and addition method. La_2O_3 was used mainly as basic

additive to control surface acidity of alumina [29,32,34,35,39,41], and was here proposed as bulk support. The recipe for FP synthesis was optimized on the basis of previous investigations for the preparation of mixed oxides [43–46]. We have chosen propionic acid as main solvent for the dissolution of the precursor salts in the case of lanthana supported samples, whereas we used xylene for the dissolution of the Ti precursor. Xylene was in any case added 1:1 also to the mother solution based on propionic acid to increase flame temperature, and the concentration of the solution was optimized with liquid flowrate to get a suitable compromise between productivity and surface area [45].

An estimate of flame temperature based on IR thermograms when using propionic acid/xylene mixtures under the present synthesis conditions has been reported elsewhere [46]. Here we can roughly estimate a flame temperature *ca*. 1000 °C in the core of the main flame.

3.1. Textural, structural and morphological characterization

The composition and synthesis method for all the samples are summarised in Table 1.

The samples were characterized by different specific surface area (SSA), depending on the support. SSA was 84 and 41 m^2/g for TiO_2 and La_2O_3, respectively. After deposition of the active phase by impregnation the SSA dramatically decreased. By contrast, samples made directly by FP showed SSA comparable with the respective support in the case of La_2O_3-based samples. This is not surprising since impregnation may occlude part of the porosity of the sample, whereas the one-pot introduction of Ni during the synthesis in principle should not affect the textural properties of the sample. By contrast, SSA decreased by *ca*. 20-30% with respect to the bare support in the case of the TiO_2-supported catalysts prepared one pot by FP because a macroscopic structural modification occurred passing from anatase (Ti-F) to rutile (X-Ni/Ti-F), as described below.

EDX analysis allowed to check catalysts composition. The results show a higher atomic ratio of Ni/La with respect to Ni/Ti for both the FP-made and impregnated samples, as expected from nominal composition. However, the samples prepared in one step by FP were characterized by lower Ni/(La,Ti) ratios than those prepared by impregnation. EDS analysis is not properly a surface-sensitive tool, but it does not have high in-depth sensitivity. In this light, we can conclude higher surface exposure obtained by impregnation of the active phase than by one step synthesis. This in turns means a higher Ni dispersion into the support matrix for the FP-prepared samples. Furthermore, due to high stability of the $LaNiO_3$ mixed oxide, it is hard to keep NiO segregated on the surface when supported over La_2O_3.

The TiO_2 sample showed a highly crystalline structure composed of rutile and anatase, the latter being the main component (Fig.1), whereas La_2O_3 was constituted by the highly hydrated form $La(OH)_3$, only. Ni addition during the FP synthesis modified the crystal structure of the support and rutile became the predominant phase (Fig.1), the only one after sample activation by reduction at 800°C. Similar results were achieved for the impregnated samples and at different Ni loading (Fig. 2). We did not get significant evidence of reflections attributed to Ni oxides or metallic Ni in the fresh samples (Fig. 2*a*), whereas Ni reflections appeared in the activated samples (Fig. 2*b*) and their intensity increased as expected with loading. Furthermore, metal dispersion was higher in the case of the samples prepared one-pot by FP than for the impregnated ones. This feature can be important to improve resistance to coking. Indeed, the modification of the structure around the Ni species plays a key role for the development of durable and stable Ni catalysts with lower C deposition and Christensen et al. [51] demonstrated the importance of the crystallite size of Ni for the steam reforming of methane.

After the addition of the active phase to the FP made lanthana, a lot of new reflections appeared that could be attributed to NiO, mainly as mixed oxide with the support: La_2NiO_4, NiO/La_2O_3 or $LaNiO_3$ (Fig. 2). After reduction, $La(OH)_3$ became the main phase, even with

$LaNiO_3$, while La_2NiO_4 almost disappeared and reflections of metallic Ni became more intense. The formation of a mixed oxide may be helpful to keep the metal well dispersed on the support, thus limiting the coking activity.

SEM micrographs (Fig. 3) of all the samples show that they were composed of uniformly sized agglomerates (*ca.* 50 nm). The primary particles were much smaller as observed by TEM analysis (Fig. 4), but different depending on the support and preparation method. The lanthana support was constituted by uniform nanoparticles, *ca*. 20-40 nm in size, but the high hydration degree (see XRD) induced agglomeration during impregnation, as testified by the TEM picture of sample 5-Ni/La-I. Similar images were obtained at higher Ni loading. This phenomenon was not observed for the sample synthesized in one step (e.g. 5-Ni/Ti-F in Fig. 4). On the contrary, a bit smaller (15-30 nm) and uniform particle size was observed for all the TiO_2 supported samples, irrespectively of the Ni loading and preparation method.

TPR analysis was made to determine the reduction temperature of Ni ions for each sample. As reported in previous investigations, this parameter was an important indication of the metal-support interaction strength. In particular, for a given metal and support couple, the highest the reduction temperature, the strongest the metal support interaction and/or the metal dispersion. Smallest particle size was also previously correlated to a lowest coking rate [25–28,36].

TPR patterns of significant samples are reported in Fig. 5-7. The H_2 consumption pattern of 15 wt%Ni supported over TiO_2 and La_2O_3 is reported in Fig. 5 for differently prepared catalysts. Lower reducibility, *i.e.* higher reduction temperature, was observed for the FP prepared samples with respect to the impregnated ones. This is commonly ascribed to higher dispersion, which is indeed imparted by the one pot synthesis with respect to impregnation. Higher reducibility characterized the TiO_2 supported samples, with respect to the lanthana-based ones, especially when prepared by impregnation. This denotes a

stronger metal-support interaction between NiO and La_2O_3, in case also leading to a mixed oxide formation (harsher reducibility), as observed indeed by XRD.

Increasing metal loading determines increasing H_2 consumption, but substantially similar reduction temperature in the case of the impregnated samples (Fig. 6 and 7). This denotes a quite similar NiO dispersion, which is expected to be reasonably low due to relatively high loading on supports with moderate surface area.

By contrast, the one pot synthesis led to slightly higher reduction temperature with increasing Ni loading. This was ascribed to the formation of an increasing amount of mixed oxide, as detected also by XRD.

3.2. Catalytic activity for the ESR – High temperature testing

All the catalysts tested at 750 °C showed full ethanol conversion and negligible formation of carbon deposits, as testified by the C balance *ca.* 100% (Table 2). The blank test evidenced marked thermal conversion of ethanol at this temperature, but it predominantly induced ethanol dehydrogenation to acetaldehyde.

The FP-prepared samples were usually characterized by higher H_2 productivity due to slightly higher water conversion. The reason can be searched in the intimate contact between the metal particles and the support, which is responsible of water activation. Thus, a more dispersed active phase can enhance the utilization of activated oxydrils and hydrogen species to complete ethanol conversion into reformate gas. The superior catalytic activity of the FP samples is also evident for the steam reforming of methane. In this context, methane is formed by ethanol decomposition and its reforming is favored by the good Ni dispersion here achieved, as evidenced by XRD and TPR. High metal loading is needed with the impregnated samples to achieve complete methane conversion, whereas no methane outflow was observed with the FP prepared samples even at low metal loading,

except for sample 15-Ni/La-F. The higher Ni dispersion and metal support interaction may account also for this point.

Overall, the H_2 productivity ranged between 1.7 and 2.3 mol/min g_{cat}. This can be further improved by adding water gas shift reactors to convert CO. Assuming the use of the reformate to feed a fuel cell with *ca*. 40% efficiency towards electrical energy, the catalyst amount needed to feed a 5 kW_{el} fuel cell would be 1.35-1.8 kg. This is a conservative estimation without taking into account the additional H_2 production through water gas shift reactors, usually connected in series to the reformer for H_2 purification before feeding the fuel cell. This amount of catalyst is competitive with literature reports for demonstrative units of such size [52–56]; catalyst volume is *e.g*. reported as 1.8 L for a methanol reformer [54].

3.3. Catalytic activity for the ESR – Low temperature testing

With the aim of process intensification, it is desirable to lower the steam reforming temperature to limit the heat load to the reactor [14,57,58], but at such low temperature coke accumulation is not effectively counter balanced by its removal by steam gasification [59,60]. This may induce rapid catalyst deactivation by formation of encapsulating coke or carbon nanofilaments [61]. The C balance is an effective parameter to monitor possible coke accumulation under these reaction conditions, as extensively described elsewhere [62].

The results of activity testing at 500 °C are summarised in Table 3. The blank test revealed limited ethanol conversion at this temperature in the absence of any catalyst. The major product also in the present case was acetaldehyde.

Both the FP and impregnated catalysts prepared over lanthana with the lowest Ni loading (5-10 wt%) do not reach a satisfactory ethanol conversion. Non negligible selectivity to acetaldehyde was also observed, together with incomplete methane reforming, overall depressing H_2 productivity.

C balance (blank test at 500°C returned 91 ± 4 %) was generally higher for the FP prepared samples, coupled with a good durability with time-on-stream. As above mentioned this is ascribed to the higher dispersion of Ni and its strong metal-support interaction. High Ni loading is needed to attain full ethanol conversion and no C_2 byproducts in the outlet gas at such a low reaction temperature.

By comparing the two supports, contrasting effects were evident. On one hand, TiO_2 usually led to higher activity (*i.e*. superior ethanol conversion, lower selectivity to acetaldehyde and methane) [63]. On the other hand, the different acid-base character of the support and different ability to disperse and stabilize the active phase induced a remarkable difference in the resistance towards coking, La_2O_3 being much more preferable from this point of view since it exhibits excellent stability with time-on-stream. The motivation of the higher C balance in the case of lanthana supports is primarily due to its basic character. The addition of lanthanum to modify a CoO_x catalyst under SRE have exhibited a significant reduction of deposited coke over the active phase to prolong the lifetime of the catalyst. We also observed higher Ni dispersion when supported over La_2O_3, especially when prepared by FP. This is another reason for higher resistance to coking, inhibiting in this case the formation of C nanofilaments due to the smaller Ni particle size. In this sense, the excessive Ni loading achieved with $LaNiO_3$ was detrimental for coking activity. Indeed, in spite of the 1:1 ionic dispersion in the precursor, after activation the high Ni concentration led to unavoidable decrease of dispersion. This in turn determined an unsatisfactory C balance.

It can be overall concluded that, based on the highest C balance and H_2 productivity, the best performing sample at 500°C was 15-Ni/La-F. Stable activity was confirmed for at least 8 h-on-stream (Fig. 8). Non negligible selectivity to methane was a drawback, which may be limited by energetically valorising this byproduct. Indeed, if the produced reformate is used in a fuel cell with typical 75% fuel utilisation (usually reported for PEM fuel cells [6452]), the byproduct methane, together with the spent reformate exiting the fuel cell, can be used

to heat up the steam reformer through a post-combustor. This would enable to improve the overall system efficiency and cost sustainability of the system. It should be also remarked that significant CO is outflowing in the reformate, imposing proper purification of H_2 according to FC purity needs. If *e.g*. a PEM FC is used, as reported elsewhere [52], max 20 ppmv CO concentration is allowed. This requires the addition of a post reforming water gas shift unit and further purification by methanation or preferential oxidation. Methanation would be preferable in this case since no additional dilution of the stream would be needed and the produced methane may be additionally valorised in the post-combustor.

Finally, the equilibrium composition (dry basis) was calculated as a function of temperature by means of the Aspen Plus software. The results are reported in Fig. 9, where the best results at 500°C and 750°C obtained with the present 15-Ni/La-F sample are superimposed. This comparison allows to conclude that the equilibrium H_2 productivity has been reached under the selected operating conditions with the best catalyst.

Finally, the present results have been compared with recent reports on SRE over Ni-based catalysts. Lanthanum oxide was used to limit alumina acidity, leading to stable Ni catalysts. However, ethanol conversion at 500°C was not complete in reports by Ma et al. [65], who used ca. 1 order of magnitude lower time factor than in the present case. Complete conversion was instead attained by Osorio-Vargas et al. [41] under conditions much similar to the present ones, although showing some byproducts. Rapid decrease of conversion (after *ca*. 4 h-on-stream) were reported elsewhere [29]. In conclusion, the present FP-prepared catalysts seem competitive with the most recent literature examples and La_2O_3 proved an interesting bulk support, not only a basic promoter for acidic oxides.

4. Conclusions

Ni-based catalysts with different metal loading and supported over lanthana or titania were synthesized and tested for the steam reforming of ethanol at different temperature. A

straightforward preparation procedure was proposed, *i.e*. flame pyrolysis, leading to high metal dispersion. This allowed to improve catalytic activity and most of all the resistance towards coking and sintering. Suitable thermal resistance was also achieved during high temperature operation. These are fundamental parameters for the practical exploitation of the process.

Satisfactory H_2 productivity was achieved at 750°C, allowing to obtain a reformate flowrate sufficient to feed a 5 kW_e fuel cell by using 1.35 kg of the best performing catalyst, as determined following a conservative estimation without taking into account further H_2 production by WGS, usually couples downstream for H_2 purification before feeding fuel cells.

Attempts of process intensification were also done by decreasing the operating temperature to 500°C. Such a temperature is very critical as for coking. The FP technique proved very effective to impart good Ni dispersion and strong metal-support interaction, thus limiting the formation of C nanotubes. The intrinsic acidity of the support has also an important role to avoid ethanol dehydration to ethylene and its consequent polymerization to form additional coke. In this respect, lanthana was much more effective than titania. However, the support played also a key role on metal dispersion. The highest dispersion was achieved over lanthana, also thanks to the formation of mixed Ni-La oxides during the one pot FP synthesis.

References

1 M. Ni, D. Y. C. Leung and M. K. H. Leung, *Int. J. Hydrogen Energy*, 2007, **32**, 3238–3247.

2 P. D. Vaidya and a E. Rodrigues, *Ind. Eng. Chem. Res.*, 2006, **45**, 6614–6618.

3 P. K. Cheekatamarla and C. M. Finnerty, *J. Power Sources*, 2006, **160**, 490–499.

4 A. Haryanto, S. Fernando, N. Murali and S. Adhikari, *Energy & Fuels*, 2005, **19**,

2098–2106.

5 G. Nahar and V. Dupont, *Biofuels*, 2012, **3**, 167–191.

6 J. Llorca, N. Homs, J. Sales and P. R. de la Piscina, *J. Catal.*, 2002, **209**, 306–317.

7 A. N. Fatsikostas and X. E. Verykios, *J. Catal.*, 2004, **225**, 439–452.

8 F. Frusteri, S. Freni, L. Spadaro, V. Chiodo, G. Bonura and S. Donato, *Catal. Commun.*, 2004, **5**, 611.

9 F. Wang, Y. Li, W. Cai, E. Zhan, X. Mu and W. Shen, *Catal. Today*, 2009, **146**, 31–36.

10 J. Y. Siang, C. C. Lee, C. H. Wang, W. T. Wang, C. Y. Deng, C. T. Yeh and C. B. Wang, *Int. J. Hydrog. Energy*, 2010, **35**, 3456.

11 H. Yoshida, R. Yamaoka and M. Arai, *Int. J. Mol. Sci.*, 2014, **16**, 350–362.

12 J. Llorca, *J. Catal.*, 2004, **222**, 470–480.

13 F. Frusteri, S. Freni, V. Chiodo, L. Spadaro, O. Di Blasi, G. Bonura and S. Cavallaro, *Appl. Catal. A Gen.*, 2004, **270**, 1–7.

14 I. Rossetti, J. Lasso, M. Compagnoni and G. De Guido, *Chem. Eng. Trans.*, 2015, **43**, 229–234.

15 A. N. Fatsikostas, D. . Kondarides and X. E. Verykios, *Catal. Today*, 2002, **75**, 145–155.

16 D. K. Liguras, K. Goundani and X. E. Verykios, *J. Power Sources*, 2004, **130**, 30–37.

17 D. Liguras, *Int. J. Hydrogen Energy*, 2004, **29**, 419–427.

18 A. Casanovas, C. de Leitenburg, A. Trovarelli and J. Llorca, *Catal. Today*, 2008, **138**, 187–192.

19 M. Domínguez, E. Taboada, E. Molins and J. Llorca, *Catal. Today*, 2012, **193**, 101–106.

20 F. L. S. Carvalho, Y. J. O. Asencios, J. D. A. Bellido and E. M. Assaf, *Fuel Process.*

Technol., 2016, **142**, 182–191.

21 J. Vicente, C. Montero, J. Ereña, M. J. Azkoiti, J. Bilbao and A. G. Gayubo, *Int. J. Hydrogen Energy*, 2014, **39**, 12586–12596.

22 A. Casanovas, M. Saint-Gerons, F. Griffon and J. Llorca, *Int. J. Hydrogen Energy*, 2008, **33**, 1827–1833.

23 a. J. Vizcaíno, P. Arena, G. Baronetti, a. Carrero, J. a. Calles, M. a. Laborde and N. Amadeo, *Int. J. Hydrogen Energy*, 2008, **33**, 3489–3492.

24 X. Hu and G. Lu, *Chem. Lett.*, 2008, **37**, 614–615.

25 I. Rossetti, C. Biffi, C. L. Bianchi, V. Nichele, M. Signoretto, F. Menegazzo, E. Finocchio, G. Ramis and A. Di Michele, *Appl. Catal. B Environ.*, 2012, **117-118**, 384–396.

26 E. Finocchio, I. Rossetti and G. Ramis, *Int. J. Hydrogen Energy*, 2013, **38**, 3213–3225.

27 I. Rossetti, J. Lasso, V. Nichele, M. Signoretto, E. Finocchio, G. Ramis and A. Di Michele, *Appl. Catal. B Environ.*, 2014, **150-151**, 257–267.

28 I. Rossetti, J. Lasso, E. Finocchio, G. Ramis, V. Nichele, M. Signoretto and A. Di Michele, *Appl. Catal. A Gen.*, 2014, **477**, 42–53.

29 C. Montero, A. Ochoa, P. Castaño, J. Bilbao and A. G. Gayubo, *J. Catal.*, 2015, **331**, 181–192.

30 J. Vicente, J. Ereña, C. Montero, M. J. Azkoiti, J. Bilbao and A. G. Gayubo, *Int. J. Hydrogen Energy*, 2014, **39**, 18820–18834.

31 J. D. a Bellido and E. M. Assaf, *J. Power Sources*, 2008, **177**, 24–32.

32 J. Bussi, N. Bespalko, S. Veiga, A. Amaya, R. Faccio and M. C. Abello, *Catal. Commun.*, 2008, **10**, 33–38.

33 K. F. M. Elias, A. F. Lucrédio and E. M. Assaf, *Int. J. Hydrogen Energy*, 2013, **38**, 4407–4417.

34 G. Garbarino, C. Wang, I. Valsamakis, S. Chitsazan, P. Riani, E. Finocchio, M. Flytzani-Stephanopoulos and G. Busca, *Appl. Catal. B Environ.*, 2015, **174-175**, 21–34.

35 a. Iriondo, V. L. Barrio, J. F. Cambra, P. L. Arias, M. B. Güemez, R. M. Navarro, M. C. Sánchez-Sánchez and J. L. G. Fierro, *Top. Catal.*, 2008, **49**, 46–58.

36 V. Nichele, M. Signoretto, F. Pinna, F. Menegazzo, I. Rossetti, G. Cruciani, G. Cerrato and A. Di Michele, *Appl. Catal. B Environ.*, 2014, **150-151**, 12–20.

37 M. C. Sánchez-Sánchez, R. M. Navarro and J. L. G. Fierro, *Catal. Today*, 2007, **129**, 336–345.

38 S. Q. Chen and Y. Liu, *Int. J. Hydrogen Energy*, 2009, **34**, 4735–4746.

39 J. Bussi, M. Musso, S. Veiga, N. Bespalko, R. Faccio and A. C. Roger, *Catal. Today*, 2013, **213**, 42–49.

40 B. Valle, B. Aramburu, A. Remiro, J. Bilbao and A. G. Gayubo, *Appl. Catal. B Environ.*, 2014, **147**, 402–410.

41 P. Osorio-Vargas, N. A. Flores-González, R. M. Navarro, J. L. G. Fierro, C. H. Campos and P. Reyes, *Catal. Today*, 2015, **259**, 27–38.

42 W. Y. Teoh, R. Amal and L. Mädler, *Nanoscale*, 2010, **2**, 1324–1347.

43 G. L. Chiarello, I. Rossetti, L. Forni, P. Lopinto and G. Migliavacca, *Appl. Catal. B Environ.*, 2007, **72**, 218–226.

44 G. L. Chiarello, I. Rossetti, L. Forni, P. Lopinto and G. Migliavacca, *Appl. Catal. B Environ.*, 2007, **72**, 227–232.

45 G. L. Chiarello, I. Rossetti and L. Forni, *J. Catal.*, 2005, **236**, 251–261.

46 G. L. Chiarello, I. Rossetti, P. Lopinto, G. Migliavacca and L. Forni, *Catal. Today*, 2006, **117**, 549–553.

47 I. Rossetti, O. Buchneva, C. Biffi and R. Rizza, *Appl. Catal. B Environ.*, 2009, **89**, 383–390.

48 E. Lim, T. Visutipol, W. Peng and N. Hotz, in *ASME 2013 7th International Conference on Energy Sustainability*, ASME, 2013, p. V001T05A007.

49 N. Hotz, in *Volume 6A: Energy*, ASME, 2013, vol. 6 A, p. V06AT07A092.

50 I. Rossetti, A. Gallo, V. Dal Santo, C. L. Bianchi, V. Nichele, M. Signoretto, E. Finocchio, G. Ramis and A. Di Michele, *ChemCatChem*, 2013, **5**, 294–306.

51 K. O. Christensen, D. Chen, R. Lødeng and A. Holmen, *Appl. Catal. A Gen.*, 2006, **314**, 9–22.

52 I. Rossetti, C. Biffi, G. F. Tantardini, M. Raimondi, E. Vitto and D. Alberti, *Int. J. Hydrogen Energy*, 2012, **37**, 8499–8504.

53 R. C. Samsun, J. Pasel, H. Janßen, W. Lehnert, R. Peters and D. Stolten, *Appl. Energy*, 2014, **114**, 238–249.

54 S. L. Sahlin, S. J. Andreasen and S. K. K??r, *Int. J. Hydrogen Energy*, 2015, **40**, 13080–13089.

55 T. Jo, J. Han, B. Koo and D. Lee, *Heat Mass Transf.*, 2016.

56 V. A. Munts, Y. V. Volkova, N. S. Plotnikov, A. M. Dubinin, V. G. Tuponogov and V. A. Chernishev, *Therm. Eng.*, 2015, **62**, 779–784.

57 I. Rossetti, M. Compagnoni and M. Torli, *Chem. Eng. J.*, 2015, **281**, 1036–1044.

58 I. Rossetti, M. Compagnoni and M. Torli, *Chem. Eng. J.*, 2015, **281**, 1024–1035.

59 S. Y. Foo, C. K. Cheng, T.-H. Nguyen and A. A. Adesina, *Catal. Today*, 2011, **164**, 221–226.

60 S. Y. Foo, C. K. Cheng, T.-H. Nguyen and A. A. Adesina, *J. Mol. Catal. A Chem.*, 2011, **344**, 28–36.

61 J. Comas, F. Mariño, M. Laborde and N. Amadeo, *Chem. Eng. J.*, 2004, **98**, 61–68.

62 S. Thaicharoensutcharittham, V. Meeyoo, B. Kitiyanan, P. Rangsunvigit and T. Rirksomboon, *Catal. Today*, 2011, **164**, 257–261.

63 A. Khataee and A. G. Mansoori, in *Nanostructured Titanium dioxide materials:*

properties, preparation and applications, Hackensack, NJ, Ed., World Scientific Publishing, 2012.

64 R. Koch, E. López, N. J. Divins, M. Allué, A. Jossen, J. Riera and J. Llorca, *Int. J. Hydrogen Energy*, 2013, **38**, 5605–5615.

65 H. Ma, L. Zeng, H. Tian, D. Li, X. Wang, X. Li and J. Gong, *Appl. Catal. B Environ.*, 2016, **181**, 321–331.

Table 1: Composition and main physical properties of the samples. SSA = specific surface area from BET regression of N_2 adsorption/desorption data. Actual Ni/Ti or La molar ratio from EDX analysis. Particle size as detected by TEM analysis.

Sample	**Composition**	**SSA (m^2/g)**	**Ni/(Ti or La) (mol/mol)**	**Ni / NiO particle size (Nm)**
Ti-F	TiO_2	84	-	-
La-F	La_2O_3	41	-	-
5-Ni/Ti-I	5wt% Ni /TiO_2	-	0.09	5 – 20
10-Ni/Ti-I	10wt% Ni /TiO_2	6.4	0.12	10 - 20
15-Ni/Ti-I	15wt% Ni /TiO_2	-	0.30	15 - 25
5-Ni/Ti-F	5wt% Ni /TiO_2	55	0.05	5 - 15
10-Ni/TI-F	10wt% Ni /TiO_2	62	0.13	5 – 15
15-Ni/Ti-F	15wt% Ni /TiO_2	53	0.16	10 - 15
5-Ni/La-I	5wt% Ni /La_2O_3	-	0.29	10 - 20
10-Ni/La-I	10wt% Ni /La_2O_3	11	0.58	25 - 35
15-Ni/La-I	15wt% Ni /La_2O_3	-	0.62	80 - 100
5-Ni/La-F	5wt% Ni /La_2O_3	48	0.12	-
10-NiI/La-F	10wt% Ni /La_2O_3	42	0.32	5 - 10
15-Ni/La-F	15wt% Ni /La_2O_3	40	0.52	5 - 15
LaNi-F	$LaNiO_3$ (Ni = 24 wt%)	11	1.09	5 - 10

Table 2: Activity testing at 750 ^{o}C, water/ethanol= 3 (mol/mol), GHSV= 2500 h^{-1}. S = selectivity. Averaged data between 4 and 8 h-on-stream.

Catalyst	**C balance (%)**	**H_2 productivity (mol/min)/ kg_{cat}**	**Ethanol Conversion (-)**	**S CH_3CHO (%)**	**S CH_4 (%)**
Blank	103 ± 3	0.061±0.006	0.54±0.04	62 ± 4	0
5-Ni/La-F	103 ± 4	1.93 ± 0.10	1.0	0	0
5-Ni/La-I	103 ± 3	1.8 ± 0.2	1.0	0	0.7 ± 0.2
5-Ni/Ti-F	105 ± 6	2.07 ± 0.14	1.0	0	0.9 ± 0.2
5-Ni/Ti-I	99 ± 3	1.7 ± 0.2	1.0	0	1.2 ± 0.3
10-Ni/La-F	100.0 ± 1.4	2.05 ± 0.03	1.0	0	0
10-Ni/La-I	102 ± 2	1.85 ± 0.02	1.0	0	1.05 ± 0.12
10-Ni/Ti-F	100 ± 3	1.40 ± 0.03	1.0	0	0
10-Ni/Ti-I	95.4 ± 1.7	1.77 ± 0.10	1.0	0	0
15-Ni/La-F	98 ± 4	1.85 ± 0.13	1.0	0	1.2 ± 0.3
15-Ni/La-I	99 ± 7	2.3 ± 0.5	1.0	0	0
15-Ni/Ti- F	100.4 ± 1.8	2.12 ± 0.14	1.0	0	0
15-Ni/Ti-I	101 ± 2	1.96 ± 0.06	1.0	0	0
LaNi-F	101 ± 7	1.9 ± 0.2	1.0	0	0

Table 3: Activity testing at 500 °C, water/ethanol= 3 (mol/mol), GHSV= 2500 h^{-1}. S = Selectivity. Averaged data between 4 and 8 h-on-stream.

Catalyst	C balance (%)	H_2 productivity (mol/min)/ kg_{cat}	Ethanol Conversion (-)	S CH_3CHO (%)	S CH_4 (%)	Max coking rate (g_C/min kg_{cat})
Blank	98 ± 4	n.d.	0.09 ± 0.03	82 ± 2	0	0
5-Ni/La-F	95 ± 8	0.88 ± 0.09	0.6 ± 0.2	12 ± 5	8.5*	0.52
5-Ni/La-I	67 ± 8	0.6 ± 0.2	0.66 ± 0.06	9.1 ± 0.5	1.3 ± 0.3	1.60
5-/Ni/Ti-F	75 ± 4	1.6 ± 0.2	1.0	0	4.8 ± 0.2	1.10
5-Ni/Ti-I	58 ± 5	1.07 ± 0.07	1.0	3.7 ± 1.4	2.3 ± 0.4	1.70
10-Ni/La-F	89 ± 2	1.18 ± 0.05	0.72 ± 0.05	7.4 ± 0.2	6.7 ± 0.3	0.49
10-Ni/La-I	93 ± 4	1.42 ± 0.07	0.97 ± 0.04	3.7 ± 0.4	9.7 ± 0.7	0.51
10-Ni/Ti-F	82 ± 8	0.90 ± 0.06	1.0	2.5 ± 0.9	3.5 ± 0.3	0.45
10-Ni/Ti-I	75 ± 8	1.4 ± 0.2	1.0	0	12.5 ± 1.6	0.41
15-Ni/La-F	95 ± 2	1.75 ± 0.02	1.0	0	9.8 ± 0.3	0.52
15-Ni/La-I	78 ± 5	1.8 ± 0.4	1.0	0	4.9 ± 1.9	0.43
15-Ni/Ti-F	61 ± 2	1.44 ± 0.05	1.0	0	3.5 ± 1.0	0.33
15-Ni/Ti-I	69 ± 3	1.67 ± 0.02	1.0	0	5.0 ± 0.6	0.38
LaNi-F	83.3 ± 0.8	1.69 ± 0.08	1.0	0	7.3 ± 0.2	0.46

* Datum based on one value only, the remaining values of selectivity being nil.

FIGURES

Fig. 1: XRD patterns of TiO_2 based samples. From bottom up: Ti, 15-Ni/Ti-F and 15-Ni/Ti-F after activation.

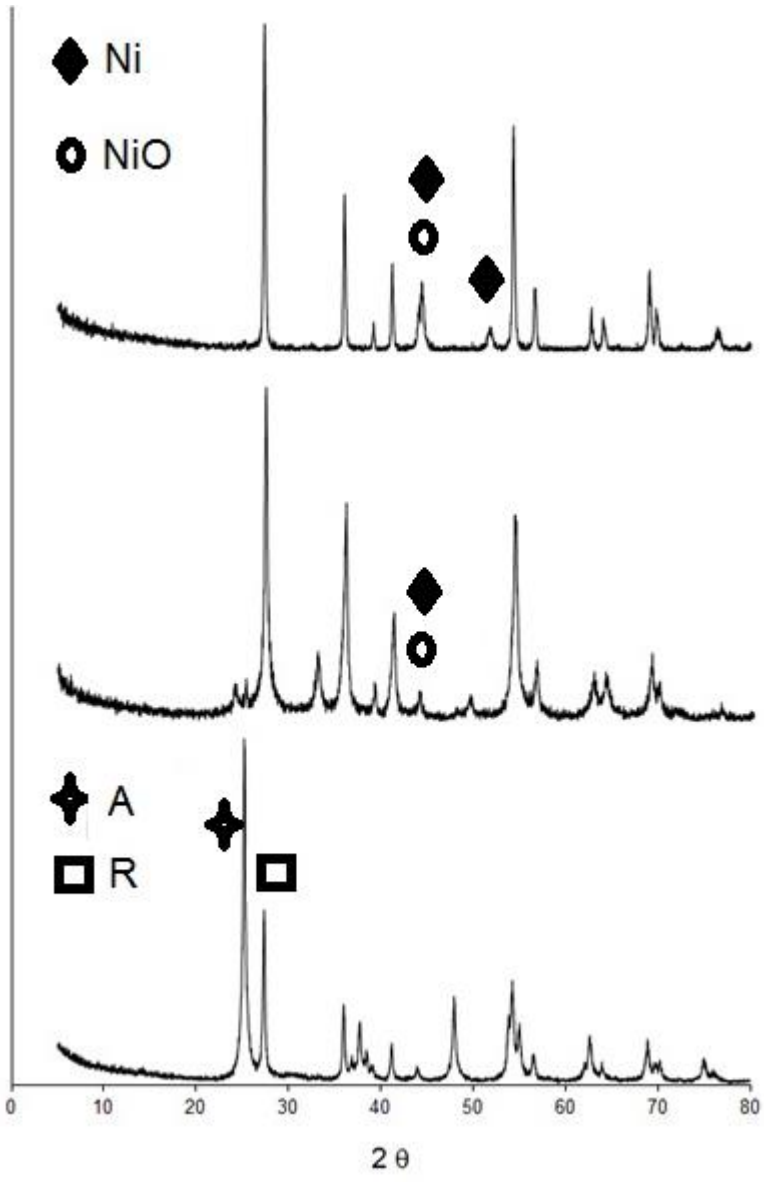

Fig. 2: XRD patterns of a) as prepared and b) activated samples. From bottom up: 10-Ni/Ti-I, 10-Ni/Ti-F, 10-Ni/La-I, 10-Ni/La-F.

a)

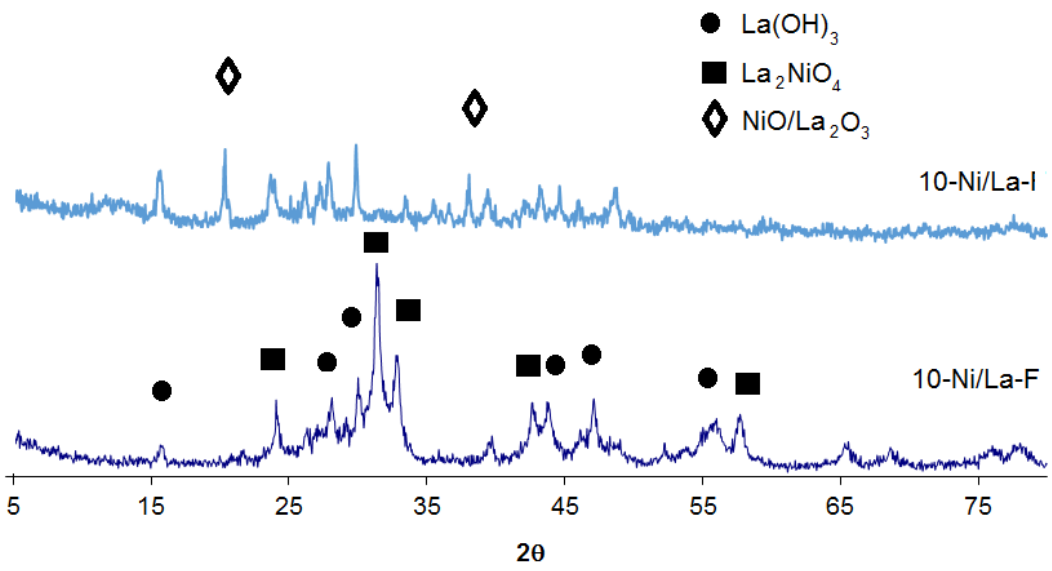

b)

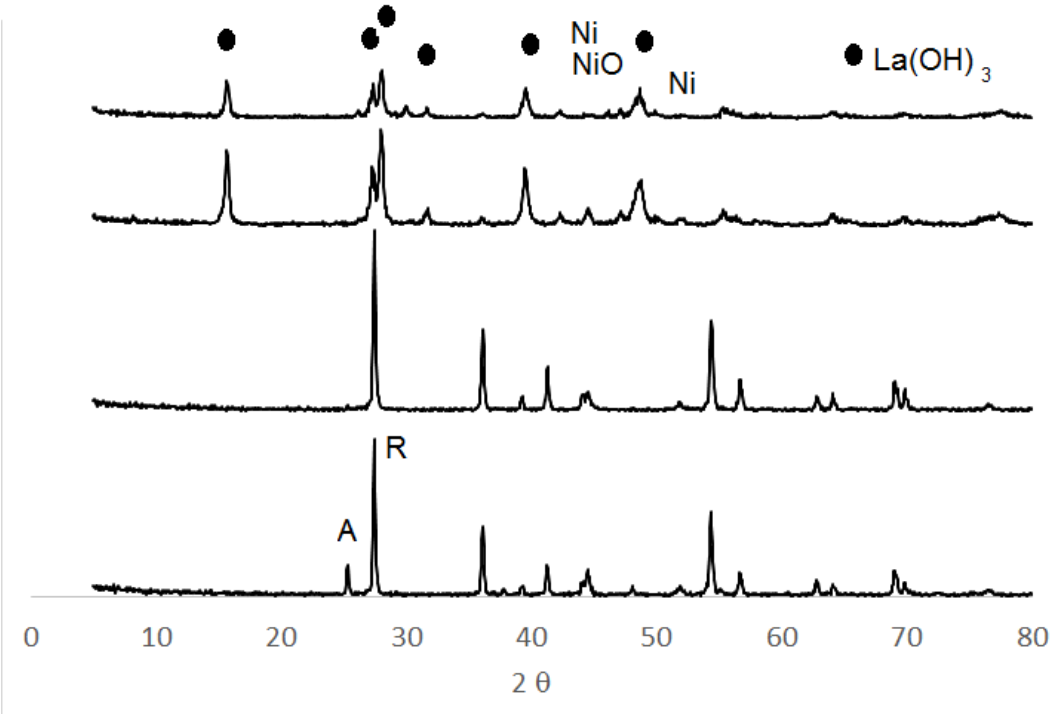

Fig. 3: Typical SEM micrographs of the FP-made samples.

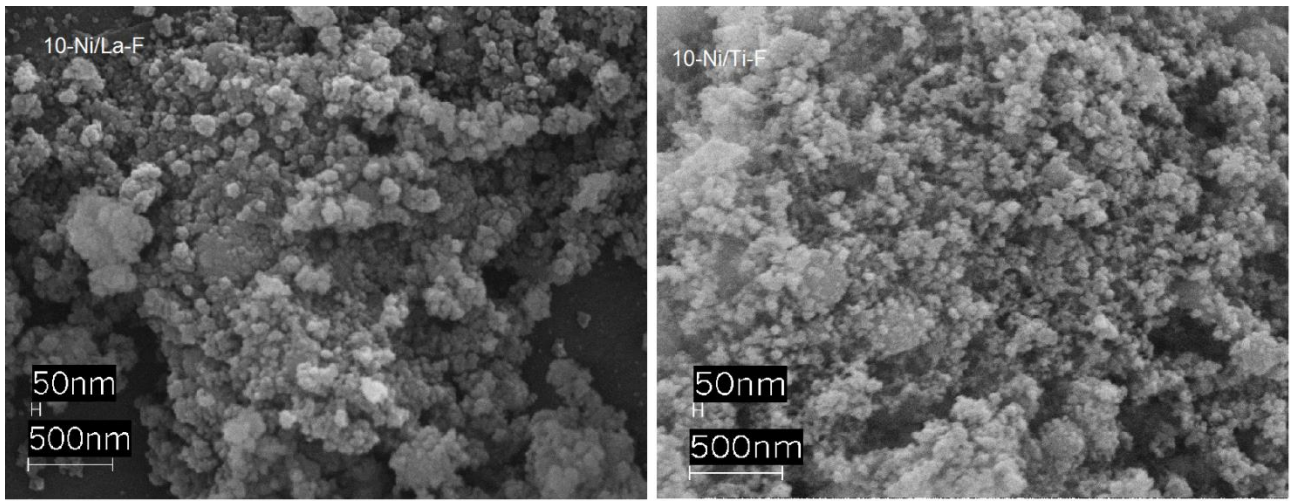

Fig. 4: TEM micrographs of selected samples. Marker size: 100 nm.

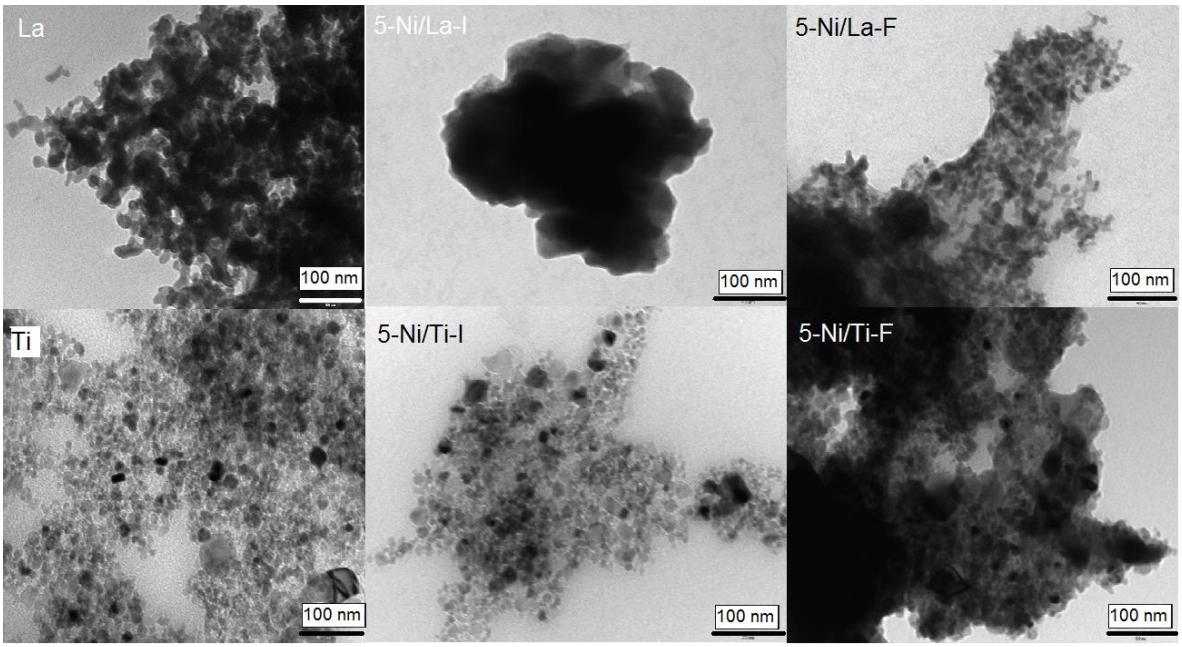

Fig. 5: TPR patterns of differently supported and prepared samples. MS signal intensity referred to H_2 consumption.

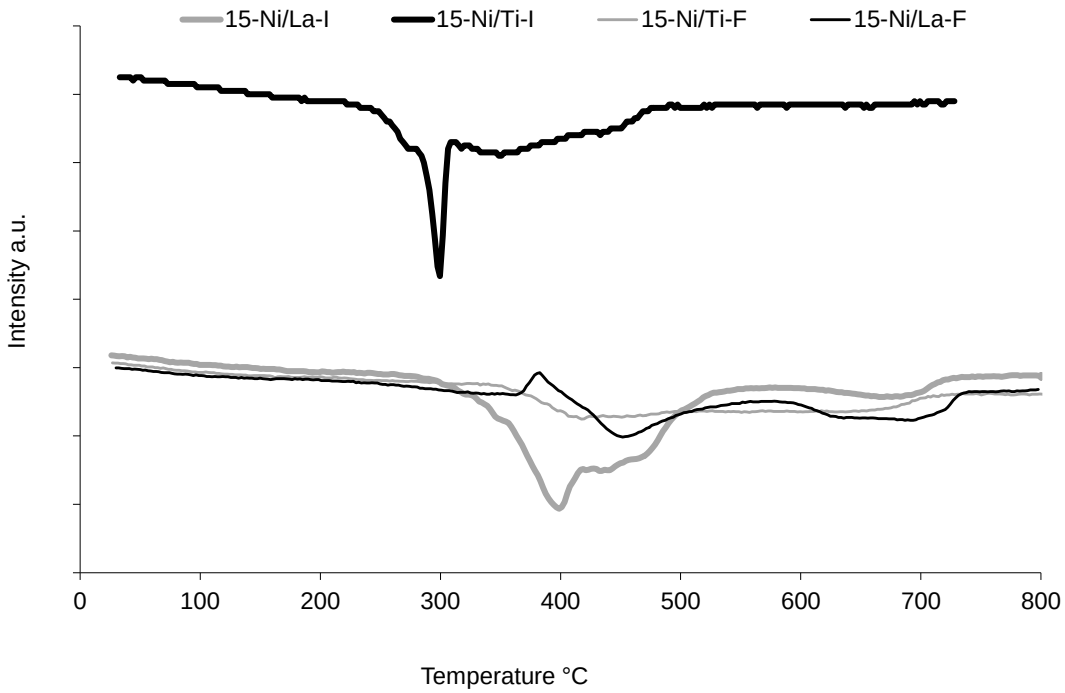

Fig. 6: TPR patterns of lanthana-supported samples prepared by FP (a) and impregnation (b). MS signal intensity referred to H_2 consumption.

a)

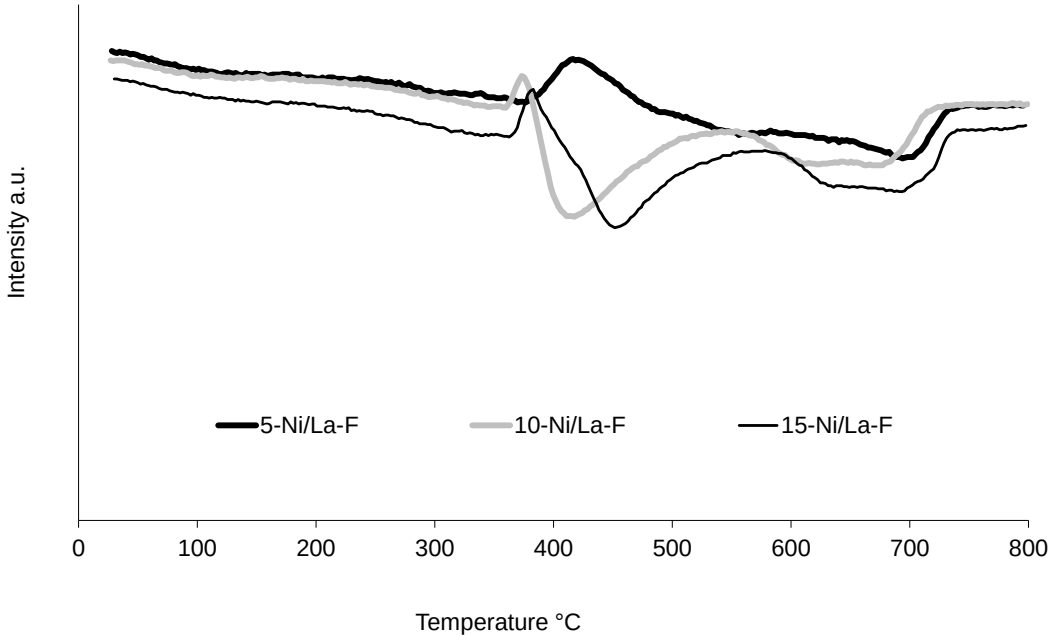

b)

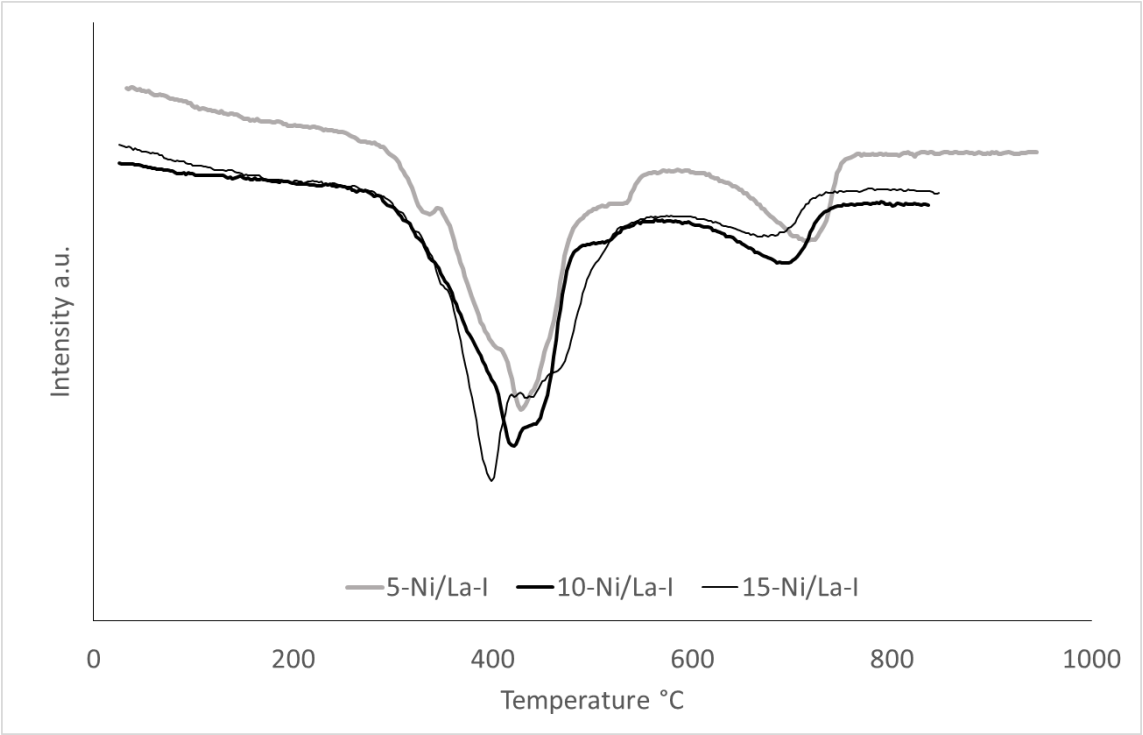

Fig. 7: TPR patterns of titania-supported samples prepared by FP (a) and impregnation (b). MS signal intensity referred to H_2 consumption.

a)

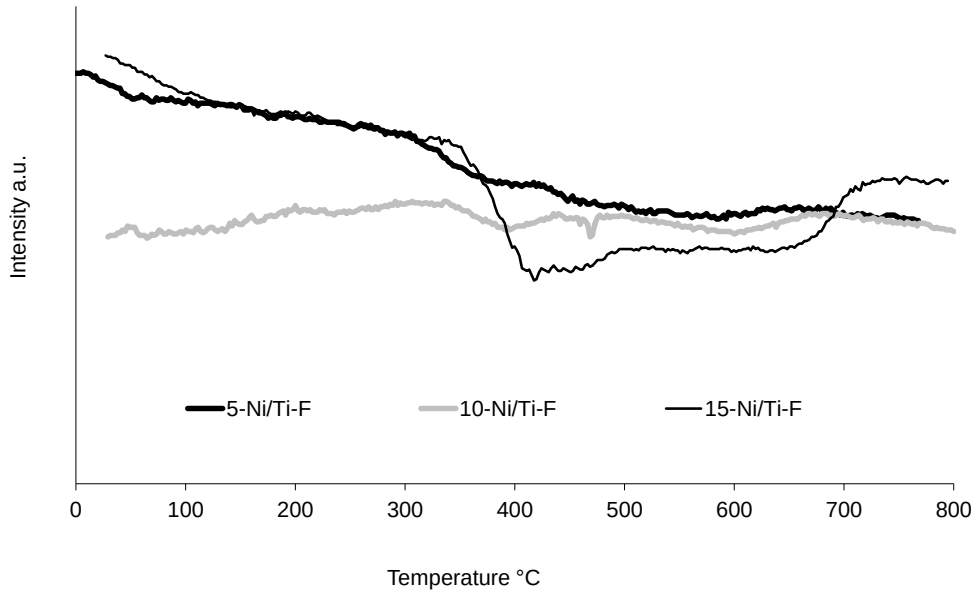

b)

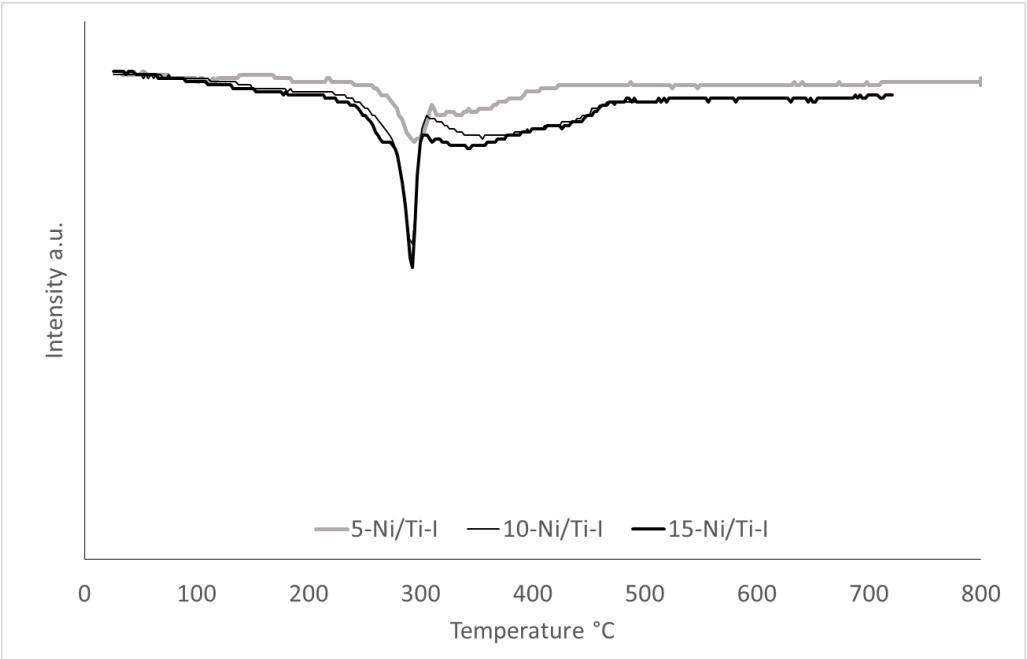

Fig.8: Sample 15-Ni/La-F tested at 500°C, performance vs. time-on-stream. a) Reactants conversion and C balance; b) products distribution (H_2 balance).

a)

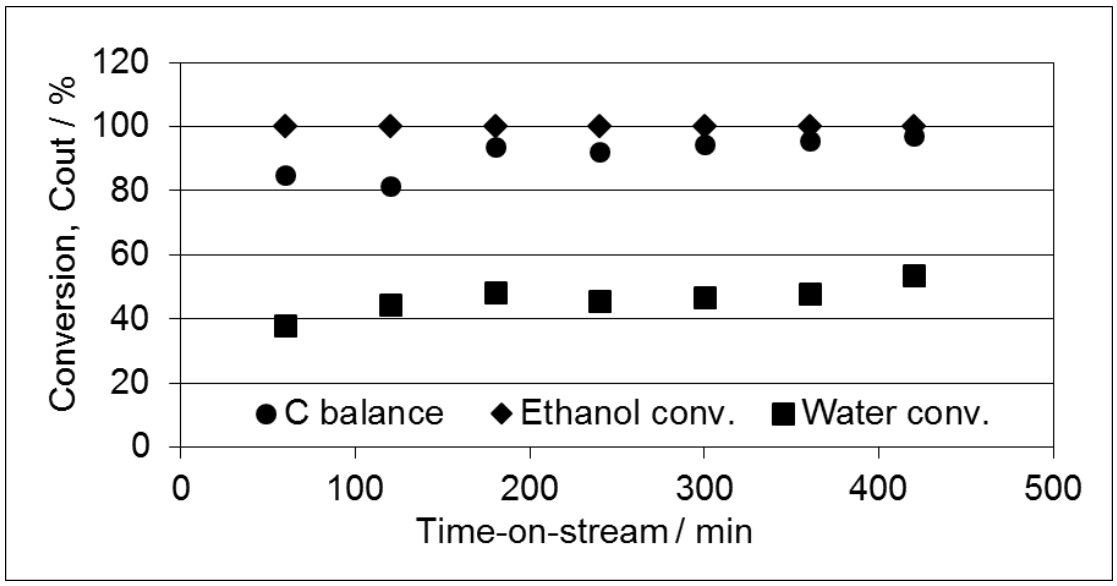

b)

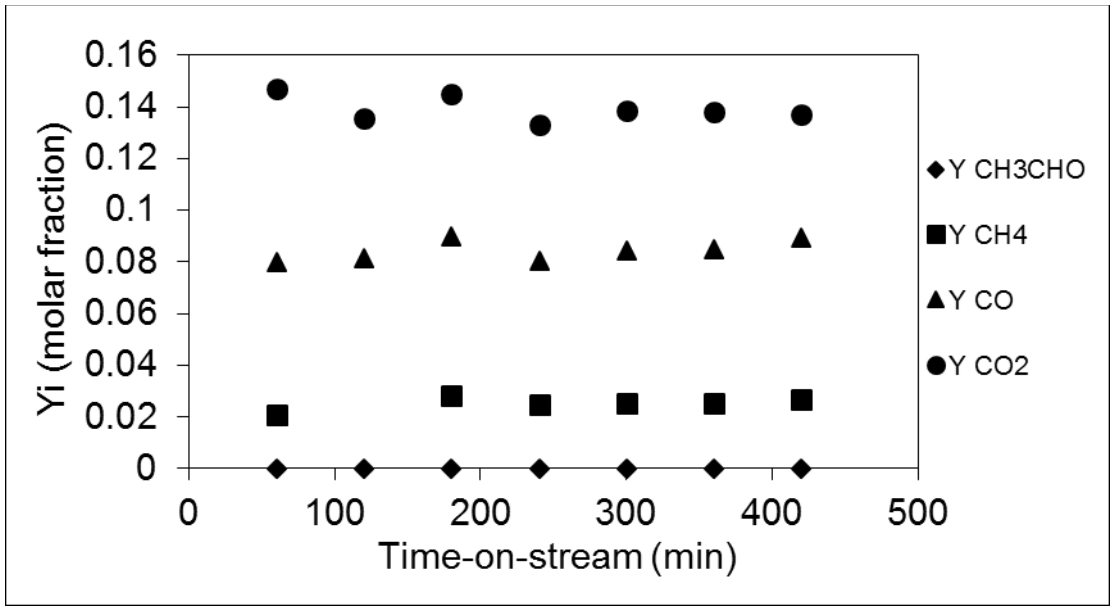

Fig.9: Equilibrium molar fractions vs. temperature (continuous lines). Markers represent experimental data obtained with sample 15-Ni/La-F. Caption of symbols: H_2 squares, CO diamonds, CO_2 x.

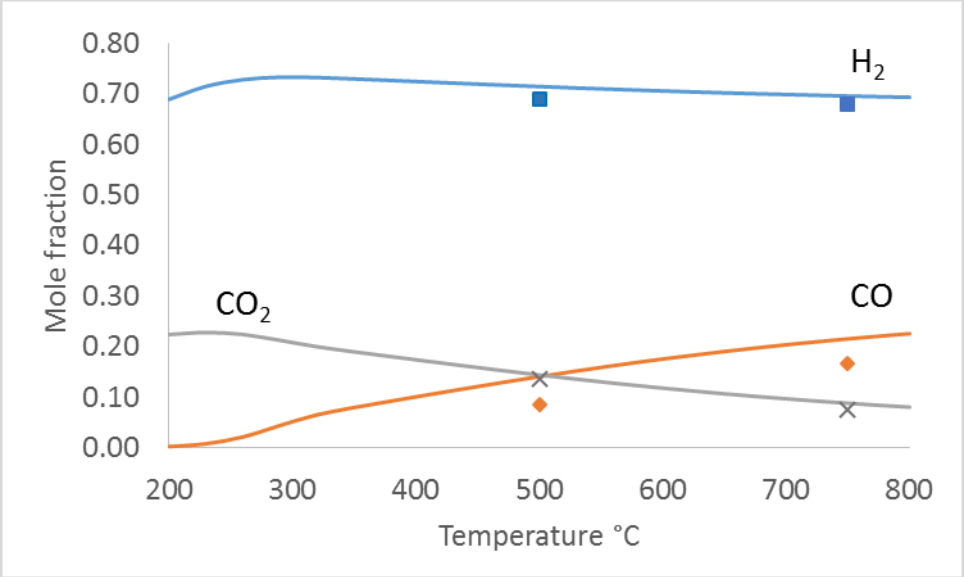

TOC

New catalysts have been prepared by flame pyrolysis for ethanol steam reforming which proved very active and stable.